

SymFET: A Proposed Symmetric Graphene Tunneling Field-Effect Transistor

Pei Zhao, *Student Member, IEEE*, Randall M. Feenstra, Gong Gu, and Debdeep Jena

Abstract—In this paper, an analytical model for calculating the channel potential and current–voltage characteristics in a symmetric tunneling field-effect transistor (SymFET) is presented. The current in a SymFET flows by tunneling from an n-type graphene layer to a p-type graphene layer. A large current peak occurs when the Dirac points are aligned at a particular drain-to-source bias V_{DS} . Our model shows that the current of the SymFET is very weakly dependent on temperature. The resonant current peak is controlled by chemical doping and applied gate bias. The on/off ratio increases with graphene coherence length and doping. The symmetric resonant peak is a good candidate for high-speed analog applications and can enable digital logic similar to the BiSFET. Our analytical model also offers the benefit of permitting simple analysis of features such as the full-width at half-maximum (FWHM) of the resonant peak and higher order harmonics of the nonlinear current. The SymFET takes advantage of the perfect symmetry of the band structure of 2-D graphene, a feature that is not present in conventional semiconductors.

Index Terms—Graphene, resonant tunneling devices, tunneling, vertical FETs.

I. INTRODUCTION

GRAPHENE is an atomically thin 2-D crystal [1]. Due to the high mobility of carriers in it, their linear dispersion, and perfect 2-D confinement, graphene is being considered as a channel material for future electronic devices. However, some challenges such as opening a finite bandgap for digital applications still remain.

A distinguishing feature of graphene is its symmetric electronic band structure. The valence band is a perfect mirror image of the conduction band about the Dirac point. Such symmetry carries over to gapped 2-D crystals such as hexagonal boron nitride (h-BN) and less so to transition metal dichalcogenides [such as molybdenum disulfide (MoS_2)] [2]. This unique band

structure *symmetry* has not been sufficiently exploited for active device applications to date.

Most studies of graphene-based devices have focused on carrier transport in the 2-D plane of the crystal. Recently, however, carrier transport *out of the plane*, i.e., vertical to the graphene sheet, has received increased attention. These studies of out-of-plane charge transport in 2-D crystals have been motivated by the proposal of the bilayer pseudospin field-effect transistor (FET) (BiSFET) in 2009 [3]. The BiSFET exploits the fact that two graphene layers can be placed in close proximity and, if populated by electrons and holes, the strong Coulomb attraction between them can lead to exciton formation. Excitons are bosonic quasi-particles and can undergo condensation below a certain critical temperature. Since the Fermi degeneracy in graphene is tunable over a large energy window, the critical temperature for the excitonic condensate has been calculated to be higher than room temperature. The formation of the excitonic condensate is expected to lead to a macroscopic tunneling current between the layers. Similar behavior has been observed at low temperatures and at high magnetic fields in coupled AlGaAs/GaAs electron–hole bilayers [4], [5]. Thus, the BiSFET has the potential to realize many-body excitonic tunneling phenomena at room temperature. The power dissipation in computing using the functionality of BiSFET is predicted to be many orders lower than conventional CMOS switching.

Stacking of different 2-D crystals leads to a novel class of heterostructures [6]. For example, stacking graphene with BN results in a smooth surface, since BN shares the same hexagonal lattice structure with graphene. The absence of out-of-plane covalent bonds implies that strain effects in similar lattice-mismatched heterostructures based on sp^3 -bonded 3-D crystals are much reduced or, perhaps, even eliminated. At low carrier concentration $n \sim 10^{11} \text{ cm}^{-2}$, the device exhibits mobilities on the order of $100\,000 \text{ cm}^2/\text{V} \cdot \text{s}$ at room temperature, which are much higher than those for graphene on SiO_2 or SiC [7]. Electron transport *out of the plane* of graphene has also started receiving attention in experiments. For example, a graphene/BN/graphene sandwich heterostructure was recently reported [8], and interlayer electron transport was measured. This stacked graphene/BN/graphene heterostructure showed a room-temperature switching ratio of 50 and 10 000 for a similar graphene/ MoS_2 /graphene structure [8]. Another recent report [9] showed that electrons can be moved from 2-D graphene into and out of silicon to form a variable-barrier-height device (the barristor).

As charge transport out of the plane of graphene receives increasing attention, a pertinent question emerges upon careful

Manuscript received September 23, 2012; revised November 28, 2012; accepted December 31, 2012. Date of publication January 25, 2013; date of current version February 20, 2013. This work was supported in part by the Semiconductor Research Corporation's Nanoelectronics Research Initiative, by the National Institute of Standards and Technology through the Midwest Institute for Nanoelectronics Discovery, and by the National Science Foundation. The review of this paper was arranged by Editor R. K. Lake.

P. Zhao and D. Jena are with the Department of Electrical Engineering, University of Notre Dame, Notre Dame, IN 46556 USA (e-mail: pzhao@nd.edu; djena@nd.edu).

R. M. Feenstra is with the Department Physics, Carnegie Mellon University, Pittsburgh, PA 15213 USA (e-mail: feenstra@cmu.edu).

G. Gu is with the Department Electrical Engineering and Computer Science, University of Tennessee, Knoxville, TN 37996 USA (e-mail: ggu1@utk.edu).

Color versions of one or more of the figures in this paper are available online at <http://ieeexplore.ieee.org>.

Digital Object Identifier 10.1109/TED.2013.2238238

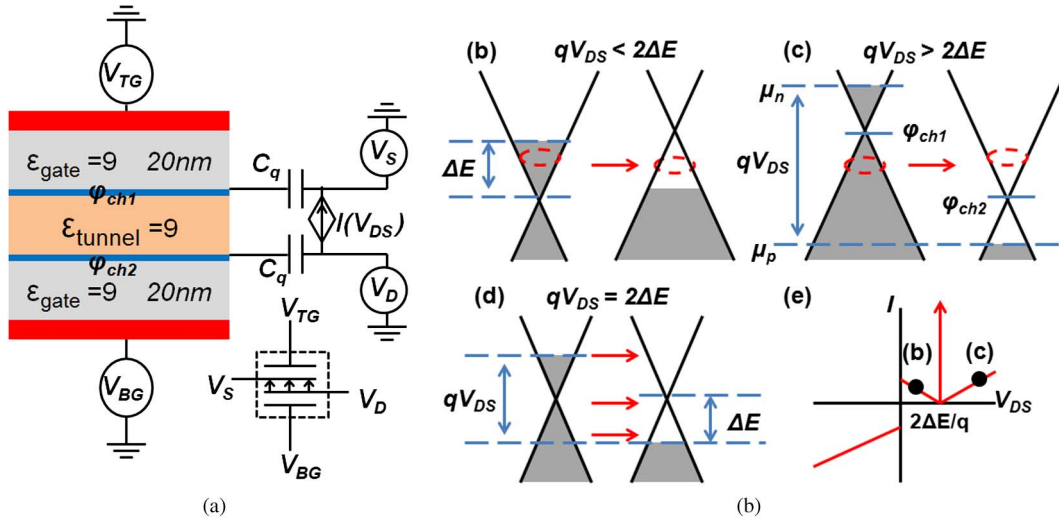


Fig. 1. (a) Sketch of the SymFET and the energy-band diagrams for a doped GIG junction at voltages of (b) $qV_{DS} < 2\Delta E$, (c) $qV_{DS} > 2\Delta E$, and (d) $qV_{DS} = 2\Delta E$. A qualitative I - V_{DS} characteristic is shown in (e). The inset in (a) shows the symbol defined for the SymFET.

analysis of the proposed BiSFET device. What is the expected behavior of a similar device structure consisting of a graphene–insulator–graphene (GIG) p-n junction heterostructure in the *absence* of the many-body excitonic condensate? Similar devices already exist in III–V resonant tunneling diodes, where single-particle tunneling itself leads to a number of interesting and useful quantum phenomena that persist at room temperature. Negative differential resistance is one such effect. Single-particle tunneling current transport has found enhanced attention recently in homo- and heterojunction tunneling FETs (TFETs). It has been measured across various semiconductor heterostructures at room temperature, highlighting its robustness [10].

One major novel feature of graphene is the perfect symmetry of the band structure, which can lead to enhanced functionality. Motivated by the above question, we recently calculated the single-particle interlayer tunneling current–voltage (I - V) curves explicitly for finite-area two-terminal GIG heterostructures [11]. The general finding was that, at most interlayer bias voltages, energy and momentum conservations force a small tunneling current to flow at one particular energy halfway between the two Dirac points. However, at a particular interlayer voltage when the Dirac points of the p- and n-type graphene layers align, a very large interlayer tunneling current flows. This is because energy and momentum are conserved in this process for all electron energies between the quasi-Fermi levels of the n- and p-type graphene layers. The I - V curve is dominated by a Dirac–delta function-like peak at the critical interlayer voltage and smaller currents at all other voltages. Our explicit calculation of the tunneling current also showed that the effect is highly robust to temperature but less robust to rotational misalignment of the two graphene layers. This surprising yet conceptually simple behavior of the two-terminal GIG device leads naturally to the following question: How will a transistor geometry with the single-particle GIG tunneling junction as its channel behave?

In this paper, we extend the detailed physical model of the two-terminal GIG device described in [11] to a Symmetric

graphene tunneling FET, which we call the “SymFET” since its unique characteristics derive from the symmetry of the band structure. We derive analytical expressions for the channel potential and I - V characteristics of the SymFET. Possible logic and high-frequency applications are also discussed.

II. DEVICE MODEL

We assume a symmetric device structure as shown in Fig. 1(a). Two graphene layers are separated by an insulator, and this GIG structure is sandwiched between a top and a bottom gate. Ohmic contacts are formed to the two graphene layers, individually representing the source (S) and the drain (D). The top- and bottom-gate voltages V_{TG} and V_{BG} control the quasi-Fermi levels μ_n and μ_p in the top and bottom layers of graphene, respectively. The gate insulator thicknesses of both gates are assumed to be the same. The quasi-Fermi level is ΔE above the Dirac point in the n-type graphene layer and below the Dirac point in the p-type graphene layer. This is indicated in Fig. 1(b)–(d). The top and back gates are symmetric $V_{TG} = -V_{BG}$, and the drain–source voltage is $V_{DS} = V_D - V_S$. The inset in Fig. 1(a) shows the proposed device symbol for the SymFET.

As shown in Fig. 1(b) and 1(c), under S/D biases when the two Dirac points are misaligned, only a single energy (and lateral k -momentum ring) in the Dirac cone meets the requirement of simultaneous energy and momentum conservation, and thus, the tunneling current is small. At $V_{DS} = 2\Delta E/q$, however, the two Dirac points align, and electrons at *all* energies between the quasi-Fermi levels satisfy energy and momentum conservation. A large tunneling current is thus expected; a resonant current peak originating from the perfectly symmetric band structure of the graphene layers should result. Since graphene is not a metal, a part of the applied voltage will drop in the graphene layer itself. This effect of the finite density of states (DOS) is captured in the quantum capacitance of graphene and is included in the model. This is critical since the gate capacitance $C_g = \epsilon_g/t_g$ and the tunneling capacitance $C_t = \epsilon_t/t_t$ are large

and can reach the quantum capacitance limit easily [12]. For simplicity of calculation, we use the $T \rightarrow 0$ K limit for quantum capacitance

$$C_q = \frac{2}{\pi} \frac{|\Delta E|}{(\hbar v_F/q)^2} \quad (1)$$

where q is the single electron charge, v_F is the Fermi velocity in graphene, and \hbar is the reduced Planck constant. It can be verified that this approximation is a good one at room temperature.

The source and drain electrodes are assumed to be perfect ohmic contacts for simplicity. In practice, the contact resistance will also force a voltage drop and can be added on top of the intrinsic model. The interlayer tunneling current calculated in [11] depends on the interlayer voltage difference. Therefore, to find the behavior of the four-terminal SymFET, the potentials of the two graphene layers φ_{ch1} and φ_{ch2} need to be identified as a function of the gate and drain/source biases (the channel potentials of graphene and Fermi levels are referenced to the aligned channel potentials at flatband). To do so, we invoke the charge neutrality condition

$$\left(\frac{\varphi_{\text{ch1}}}{q} + V_{\text{TG}}\right) C_g + \left(\frac{\varphi_{\text{ch1}}}{q} - \frac{\varphi_{\text{ch2}}}{q}\right) C_t + \left(\frac{\varphi_{\text{ch1}}}{q} - \frac{\mu_n}{q}\right) C_q/2 + qN = 0 \quad (2)$$

$$\left(\frac{\varphi_{\text{ch2}}}{q} + V_{\text{BG}}\right) C_g + \left(\frac{\varphi_{\text{ch2}}}{q} - \frac{\varphi_{\text{ch1}}}{q}\right) C_t + \left(\frac{\varphi_{\text{ch2}}}{q} - \frac{\mu_p}{q}\right) C_q/2 - qN = 0 \quad (3)$$

where $V_{\text{TG}} = -V_{\text{BG}} = V_G$, $N = \Delta E_{\text{doping}}^2/\pi(\hbar v_F)^2$ is the chemical doping concentration, and we assume that the work functions of the metals are matched with the undoped graphene sheets, which gives the flatband conditions at zero gate bias. The factors 1/2 in the third terms of (2) and (3) are due to the linear dependence on ΔE in the graphene quantum capacitance, which is a differential capacitance.

Then, taking (2) minus (3) and using the relationships $qV_{\text{DS}} = 2\Delta E + \varphi_{\text{ch1}} - \varphi_{\text{ch2}}$, $qV_{\text{DS}} = \mu_n - \mu_p$, $\mu_n - \varphi_{\text{ch1}} = \Delta E$, and $\varphi_{\text{ch2}} - \mu_p = \Delta E$, we can form a quadratic equation with the only unknown parameter ΔE

$$\left(V_{\text{DS}} - 2\frac{\Delta E}{q} + 2V_G\right) C_g + 2\left(V_{\text{DS}} - 2\frac{\Delta E}{q}\right) C_t - \frac{2q\Delta E^2}{\pi(\hbar v_F)^2} + 2qN = 0 \quad (4)$$

and the solution is

$$\begin{aligned} & \Delta E(V_G, V_{\text{DS}}) \\ &= -\frac{(2C_t + C_g)\pi(\hbar v_F/q)^2}{2} \\ &+ \left\{ \frac{(2C_t + C_g)^2\pi^2(\hbar v_F/q)^4}{4} + \frac{\pi(\hbar v_F)^2}{2q} \right. \\ &\left. \times [(V_{\text{DS}} + 2V_G)C_g + 2C_tV_{\text{DS}} + 2qN] \right\}^{\frac{1}{2}}. \quad (5) \end{aligned}$$

The electrostatic model used here is based on a 1-D approximation, ignoring the intra-graphene-layer potential distribution and current flows. A more rigorous treatment requires the solution of the 2-D Poisson equation, which is suggested for future work.

The analytical expression for the interlayer tunneling current at zero temperature was derived in [11]. When the Dirac points in the two graphene layers are misaligned, the nonresonant tunneling current is

$$I = G_1 \left(\frac{2\Delta E}{q} - V_{\text{DS}} \right), \quad (0 < qV_{\text{DS}} < 2\Delta E) \quad (6)$$

$$I = G_1 \left(V_{\text{DS}} - \frac{2\Delta E}{q} \right), \quad (qV_{\text{DS}} > 2\Delta E \text{ or } qV_{\text{DS}} < 0) \quad (7)$$

where the prefactor conductance $G_1 = (q^2 A/2\hbar)(\hbar\kappa u_{12}^2 e^{-\kappa t}/mdv_F)^2$, κ is a decay constant for the tunneling current in the barrier, m is the free electron mass, d is the normalization constant for the z -component wavefunction in graphene, u_{12} is a constant of order unity, and $A = L^2$, with L being the coherence length of graphene (size of ordered areas in graphene film). In this paper, we assume that the graphene size is A with coherence in all areas.

The resonant current is a perfect Dirac-delta function at $qV_{\text{DS}} = 2\Delta E$ for infinitely wide graphene sheets. For finite widths of length L , it is broadened to [11]

$$I = \frac{1.6}{\sqrt{2\pi}} G_1 \frac{L\Delta E^2 (2u_{11}^4 + u_{12}^4)}{u_{12}^4 q\hbar v_F} \times \exp \left[-\frac{A}{4\pi} \left(\frac{qV_{\text{DS}} - 2\Delta E}{\hbar v_F} \right)^2 \right] \quad (8)$$

where u_{11} is a constant of order unity similar to u_{12} . The total current is the combination of (6) or (7) and (8).

Equations (6)–(8) were derived assuming zero temperature. At finite temperature, to capture the thermal occupation of states, the current needs to be calculated by including the Fermi-Dirac distributions in the integral over all states [11]. Equations (9) and (10) are the finite-temperature expressions corresponding to (6) and (7) derived by a direct extension of the theory in our previous work [11]

$$I = G_1 \frac{4\hbar^2 v_F^2}{q} \int_0^{+\infty} \{k [f(E_{n,k} - \mu_n, T) - f(E_{p,k} - \mu_p, T)] \times \delta(2\Delta E - qV_{\text{DS}} - 2\hbar v_F k)\} dk \quad (9a)$$

$$= G_1 \left(\frac{2\Delta E}{q} - V_{\text{DS}} \right) \times [f(-qV_{\text{DS}}/2, T) - f(qV_{\text{DS}}/2, T)] \quad (9b)$$

$$= G_1 \left(\frac{2\Delta E}{q} - V_{\text{DS}} \right) \tanh \left(\frac{qV_{\text{DS}}}{4k_B T} \right), \quad (qV_{\text{DS}} < 2\Delta E) \quad (9c)$$

$$I = G_1 \frac{4\hbar^2 v_F^2}{q} \int_0^{+\infty} \{k [f(E_{n,k} - \mu_n, T) - f(E_{p,k} - \mu_p, T)] \times \delta(qV_{DS} - 2\Delta E - 2\hbar v_F k)\} dk \quad (10a)$$

$$= G_1 \left(V_{DS} - \frac{2\Delta E}{q} \right) \times [f(-qV_{DS}/2, T) - f(qV_{DS}/2, T)] \quad (10b)$$

$$= G_1 \left(V_{DS} - \frac{2\Delta E}{q} \right) \tanh\left(\frac{qV_{DS}}{4k_B T}\right), \quad (qV_{DS} > 2\Delta E) \quad (10c)$$

where subscripts n and p refer to the n-type (top) and p-type (bottom) electrodes, respectively, and the Fermi–Dirac distribution for arguments δE and T are given by $f(\delta E, T) \equiv 1/[1 + \exp(\delta E/k_B T)]$. Following [11], for (9a), with $0 < qV_{DS} < 2\Delta E$, we have $E_{n,k} - \mu_n = \hbar v_F k - \Delta E$ and $E_{p,k} - \mu_p = -\hbar v_F k + \Delta E$, hence yielding (9b) and (9c). Those equations also hold for $qV_{DS} < 0$, with the difference between the Fermi–Dirac occupation factors changing sign. For (10a), with $qV_{DS} > 2\Delta E$, we have $E_{n,k} - \mu_n = -\hbar v_F k - \Delta E$ and $E_{p,k} - \mu_p = \hbar v_F k + \Delta E$, yielding (10b) and (10c).

A finite-temperature correction to (8) is more complicated, since that equation itself is a significant approximation [11]. Nevertheless, the dominant term in its temperature dependence can be recognized as the increased number of states available for tunneling, in the resonant situation of Fig. 1(d) with $qV_{DS} = 2\Delta E$. For this resonant situation, the Dirac points of the two electrodes are aligned at energy E_d . This number of states is given simply by

$$N_s(T) = \int_{-\infty}^{+\infty} \rho(E - E_d) [f(E - E_d - \Delta E, T) - f(E - E_d + \Delta E, T)] dE \quad (11)$$

where $\rho(E) = 2|E|/[\pi(\hbar v_F)^2]$ is the DOS per unit area of graphene. Our correction to (8) is then made by multiplying it by $N_s(T)/N_s(0)$, with $N_s(0) = 2\Delta E^2/[\pi(\hbar v_F)^2]$. Expressing the result in terms of Fermi–Dirac integrals of order 1, \mathfrak{S}_1 , we have

$$\frac{N_s(T)}{N_s(0)} = \frac{2(k_B T)^2}{\Delta E^2} \left[\mathfrak{S}_1\left(\frac{\Delta E}{k_B T}\right) - \mathfrak{S}_1\left(-\frac{\Delta E}{k_B T}\right) \right] \quad (12)$$

where $\mathfrak{S}_1(x) = \int_0^{+\infty} t/[1 + \exp(t - x)] dt$.

Equations (9) and (10), as well as the product of (8) and (12), are valid only in the limit of large L , although the L value at which the approximations break down is different for the two cases. In the former case, the dominant term in the slope of $I(V_{DS})$ at $V_{DS} = 0$ is $qV_{DS}/4k_B T$, arising from the tanh terms, and this slope becomes very large for small T values. However, the exact solution for the current [11] yields a slope that is limited by the L value. We find that simply multiplying (9) and (10) by a factor of $\tanh(LqV_{DS}/\pi\hbar v_F)$ yields a slope at that agrees very well with the exact solution, and it does not significantly affect the $I(V_{DS})$ curve elsewhere. For the product

of (8) and (12), the current from (8) is nonzero at $V_{DS} = 0$, with this discrepancy being significant only for sufficiently small L values. In this case, we find that multiplying the product of (8) and (12) by a factor of $\tanh(LqV_{DS}/2\pi\hbar v_F)$ solves this problem of the nonzero current at $V_{DS} = 0$ and produces a slope at $V_{DS} = 0$ that agrees fairly well with the exact solution. Hence, our final formula for the total current is given by

$$I = G_1 \left(V_{DS} - \frac{2\Delta E}{q} \right) \text{sgn}\left(V_{DS} - \frac{2\Delta E}{q}\right) \times \tanh\left(\frac{qV_{DS}}{4k_B T}\right) \tanh\left(\frac{LqV_{DS}}{\pi\hbar v_F}\right) + \left\{ \frac{1.6}{\sqrt{2\pi}} G_1 \frac{L\Delta E^2 (2u_{11}^4 + u_{12}^4)}{u_{12}^4 q \hbar v_F} \times \exp\left[-\frac{A}{4\pi} \left(\frac{qV_{DS} - 2\Delta E}{\hbar v_F}\right)^2\right] \times \frac{N_s(T)}{N_s(0)} \tanh\left(\frac{LqV_{DS}}{2\pi\hbar v_F}\right) \right\} \quad (13)$$

where $\text{sgn}(V_{DS} - 2\Delta E/q)$ equals 1 for $V_{DS} > 2\Delta E/q$, 0 for $V_{DS} = 2\Delta E/q$, or -1 for $V_{DS} < 2\Delta E/q$.

The single-particle tunneling model used in this work captures the relevant physics, e.g., wave function overlap (detailed derivation in [11]), even in the case of strong interlayer interactions at small insulator thicknesses. The only approximation we made is that the electronic structure (band structure) of the GIG system is the same as two noninteracting graphene sheets. We have justified the approximation as follows: Any modification to the band structure due to the interaction will be near the Dirac energy. At sufficiently high doping ΔE , the error is negligible.

III. RESULTS AND DISCUSSIONS

We present the typical I – V characteristics of the SymFET at room temperature first. The comparison of $T = 300$ K and $T = 0$ K will be discussed later. The values of the decay constant κ can be calculated from the complex band structure inside the bandgap of the insulator based on the effective mass approximation [8]. Here, we use an estimated value $\kappa = 17 \text{ nm}^{-1}$, following footnote 14 of [11]. The chemical doping level is set to be $\Delta E_{\text{doping}} = 0.1 \text{ eV}$. A finite coherence length $L = 100 \text{ nm}$ is assumed; the effect of this parameter on the on/off ratio for the device is discussed below. When the SymFET scales down to 50 nm or less, momentum conservation does not scale well with device size. The scaling limits of SymFET will be a subject of future study; the quantum confinement and quantized transverse momentum in graphene nanoribbon also need to be considered near scaling limits, as discussed in [13].

The resultant I_D – V_{DS} characteristics with varying insulator thickness are shown in Fig. 2. The tunneling insulator thickness t_t is similar as the tunneling barrier thickness in double quantum-well heterostructures [5]. As t_t increases, the resonant peak current decreases, as expected. The gate insulator can be a high- k material similar to that employed in silicon CMOS technology. In addition, 2-D materials such as BN might be a

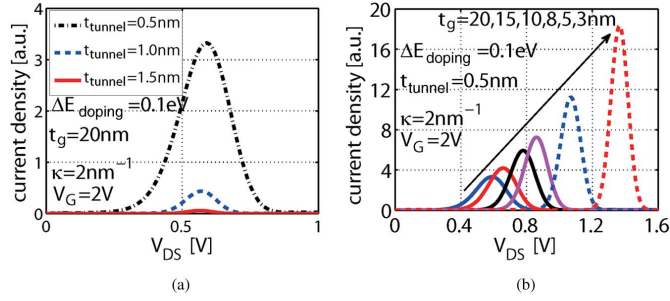


Fig. 2. I_D versus V_{DS} characteristics showing scaling with the (a) tunneling and (b) gate insulator thicknesses (an arbitrary κ value is chosen here to give a clear illustration of current density scaling).

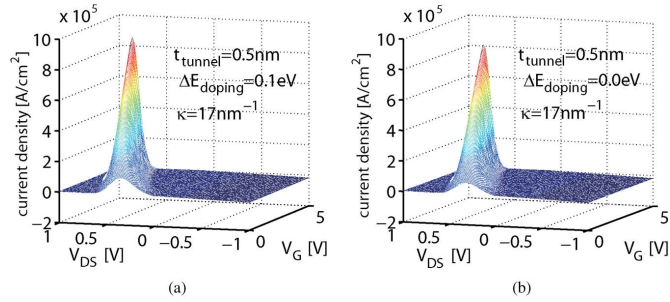


Fig. 3. Contour plot of the complete bias space for (a) chemical doping $\Delta E_{\text{doping}} = 0.1$ eV and (b) no chemical doping.

better choice to reduce the interface trap density since the dangling bond can be reduced. The measured breakdown field is as high as 7.94 MV/cm for BN [14]. Thinner t_g offers better gate control and higher gate-induced doping. When t_g decreases, ΔE becomes larger at the same gate bias. The resonant peak moves to a higher bias, and the peak current increases. For the simulation results shown next, we fix the gate capacitance with $t_g = 20$ nm and dielectric contact $\epsilon_g = 9$, tunneling insulator thickness $t_t = 0.5$ nm, and dielectric contact $\epsilon_t = 9$. (BN might have an even lower dielectric constant $\epsilon_{BN} = 3.5$ [15]).

In Fig. 3, the entire bias phase space of the I - V characteristics are shown. When the graphene sheets are chemically doped (i.e., $\Delta E_{\text{doping}} = 0.1$ eV), V_{DS} drives the carriers tunneling between the p- and n-types of graphene and the resonant peak exists for $V_G = 0$ V. With nonzero V_G , gate electrostatic doping further increases ΔE and the resonant peak shifts to a higher V_{DS} value. However, the current is quite small in the nonresonant region.

If we define the peak current as the I_{on} and the current close to $V_{DS} \sim 0$ as I_{off} , from (6) and (8), the effective on/off ratio is

$$\frac{I_{\text{on}}}{I_{\text{off}}} = \frac{0.8}{\sqrt{2\pi}} \frac{L\Delta E}{\hbar v_F}. \quad (14)$$

The effective on/off ratio is independent of temperature (ignoring the slight difference due to the Fermi tail) and increases with the doping ΔE and the graphene size L . For $L = 100$ nm, the ratio is ~ 100 and ~ 1000 for $L = 1$ μm . We also point out that the on/off ratio is not necessarily a figure of merit for the device (since the device might be employed for analog applications where high modulation is not required). In

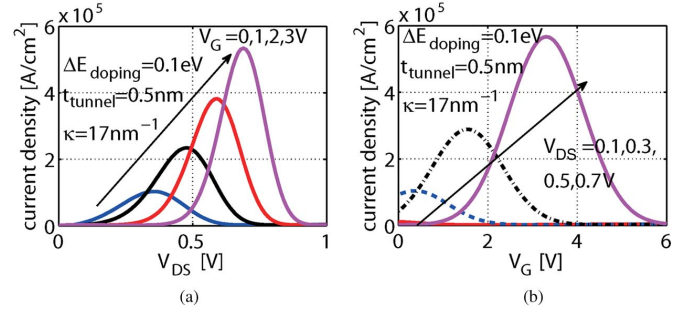


Fig. 4. (a) I_D versus V_{DS} curves with different V_G 's. (b) I_D versus V_G at different V_{DS} 's.

a similar vein, the resonant peak is symmetric in voltage and represents a rather strong negative differential resistance. The peak-to-valley-current ratio (PVCRR) of this NDR is identical to the on/off ratio defined earlier.

In Fig. 3(b), we assume that $\Delta E_{\text{doping}} = 0$ eV. At $V_G = 0$ V, ΔE is nonzero since drain bias also induces doping, similar to the case of the GIG junction in [11]. However, ΔE is small and the resonant peak is small at low V_G . When V_G increases, electrostatic doping induces an appreciable resonant current, which further increases at higher V_G .

The I_D - V_{DS} characteristics at fixed V_G is shown in Fig. 4(a). The resonant behavior shows clear ON and OFF states without a saturation region. Because we assume a chemical doping of graphene, the SymFET with a resonant current peak can operate at $V_G = 0$ V. As aforementioned, the gate will induce electrostatic doping in the graphene layer. With larger V_G , ΔE increases, the resonant condition $qV_{DS} = 2\Delta E$ occurs at larger drain bias, and the resonant current peak moves to the right. Higher V_G induces more doping and, thus, large ON-state current. In the two-terminal GIG device, the resonant current peak is proportional to the coherence length L and the width is proportional to $1/L$ [11]. In the gated SymFET, since the gate bias electrostatically dopes the graphene, it offers the additional flexibility to adjust the ON and OFF states. In Fig. 4(b), the I_D - V_G curves are shown with a strong nonlinear and resonant behavior but with wider peaks. When V_G is small and outside the resonant peak, the transconductance is small, but it is large in the peak condition.

Different from the subthreshold region of MOSFETs, we refer to the ‘‘OFF’’ state away from the resonant peak in the SymFET as the nonresonant region. Although the graphene sheets are doped, according to conservation laws, the current near $V_G = 0$ V is low [$V_{DS} = 0.7$ V, as shown by the solid line in Fig. 4(b)]. The gate voltage modulates the doping potential ΔE in SymFET. By (5), at fixed V_{DS} , doping potential ΔE is a sublinear function of V_G . The current $I_{DS}(V_G)$ at the nonresonant region roughly follows the same hyperbolic form as the first term of $I_{DS}(V_{DS})$ in (13):

$$I \propto \tanh\left(\frac{qV_G}{4k_B T}\right) \tanh\left(\frac{LqV_G}{\pi\hbar v_F}\right). \quad (15)$$

Hyperbolic functions may not offer a sharp subthreshold swing (SS), but the SymFET is more attractive for analog applications, where a steep SS is not necessary.

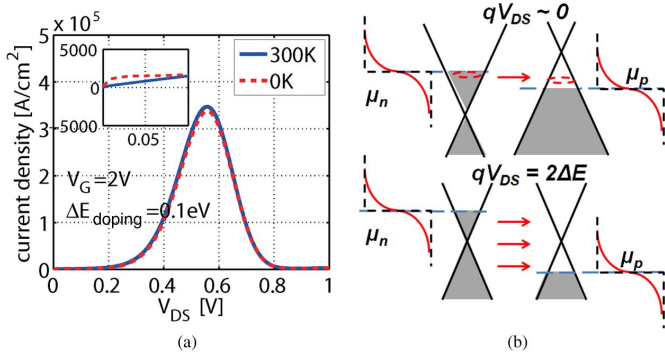


Fig. 5. (a) Comparison of I_D - V_{DS} characteristics at $T = 300$ K and $T = 0$ K. (b) Sketch of the band diagram and Fermi-Dirac distribution at $T = 300$ K and $T = 0$ K. The inset of (a) shows the current density near $V_{DS} = 0$.

The resonant current peak follows a normal distribution function $I \sim \exp(-(qV_{DS} - \Delta E)^2 / (2\sigma)^2)$, with $FWHM = 2.3548\sigma$, where $\sigma = \sqrt{2\pi\hbar v_F} / L$ for the resonant peak in SymFET. In fact, ΔE is not a constant but, instead, dependent on V_{DS} and V_G ; thus, the FWHM shown here is only an approximation. The reason for the narrower FWHM occurring for V_{DS} compared with V_G in Fig. 4 is the large gate insulator thickness (weaker gate control). A smaller FWHM of V_G can be achieved with a thinner gate insulator (not shown here).

Because tunneling is the main current transport mechanism, the I_D - V_{DS} curve is quite insensitive to temperature, as shown in Fig. 5. However, since the Fermi-Dirac distribution smears out state occupancy at a finite temperature, slight differences can still be observed between $T = 300$ K and $T = 0$ K. At low V_{DS} , the transport energy window (between the quasi-Fermi levels μ_n and μ_p) is small [Fig. 5(b)]. Then, the Fermi distribution smearing reduces the carrier density at higher temperature and the current decreases. The increase of the resonant peak current at room temperature is because of the Fermi distribution tail extending to higher energy with more states. When the Dirac points are aligned, the states at all energies conserve a lateral momentum upon tunneling and, thus, are allowed.

We note that the device current has symmetric resonances in both the I_D - V_{DS} and I_D - V_G scans. This is quite unlike what happens in a single-layer graphene FET where the “ambipolar” nature manifests itself primarily in the gate bias sweep [16], [17]. The nonlinear symmetric resonant I_D - V_{DS} behavior can be used for the purpose of frequency multiplication (Fig. 6). If a dc voltage bias at the current peak V_{DSp} is superimposed with an ac signal, the frequency of the output current will be doubled. We can use (8) to calculate the output ac signal. Assuming that $V_{DS} = V_{DSp} + v_{ds}e^{i\omega t}$, the oscillatory part of the current is

$$I = \frac{1.6}{\sqrt{2\pi}} G_1 \frac{L\Delta E^2 (2u_{11}^4 + u_{12}^4)}{u_{12}^4 q \hbar v_F} \exp\left(-\frac{A}{4\pi} \left[\frac{v_{ds}e^{i\omega t}}{\hbar v_F}\right]^2\right). \quad (16)$$

To find out the higher order harmonics, we ignore the constant prefactor

$$I \propto \exp\left(-\frac{A}{4\pi} \left[\frac{v_{ds}e^{i\omega t}}{\hbar v_F}\right]^2\right). \quad (17)$$

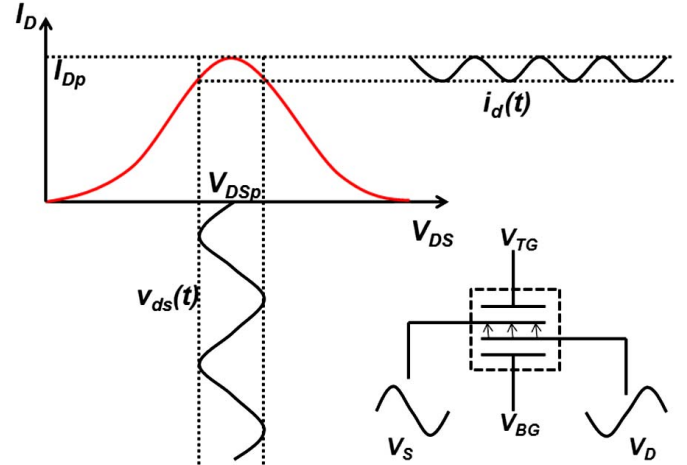


Fig. 6. Nonlinear resonant current is highly symmetric. When a dc voltage V_{DSp} biased at the current peak is superimposed with an ac signal $v_{ds}(t)$, the frequency of the output current $i(t)$ will be doubled.

This expression can be further extended as

$$I \propto 1 - C_1 \exp(2j\omega t) + \frac{C_1^2}{2!} \exp(4j\omega t) - \frac{C_1^3}{3!} \exp(8j\omega t) + \dots \quad (18)$$

where $C_1 = (A/4\pi(\hbar v_F)^2)v_{ds}^2$. In (18), only even higher harmonics occur.

The SymFET is expected to be intrinsically fast since it relies entirely on tunneling. The extrinsic performance with parasitics can be analyzed same as for any high-speed device and will not be covered in this paper. High-frequency digital operation and a host of analog applications such as frequency multiplication are thus possible by exploiting the symmetry of the band structure of 2-D graphene.

As explained in [11], the greatest amount of nonlinearity in the I - V characteristics is achieved with a nearly perfect rotational orientation of graphene layers. This presents a significant challenge in the fabrication of such devices based on the layer transfer technology. However, the epitaxial growth of graphene, BN [18], or other 2-D materials provides a choice to overcome this problem. We note that due to the many-particle nature of the excitonic condensate, the BiSFET is expected to be insensitive to rotational misalignment [3]. This is similar to the robustness of superconductivity to defects. However, the single-particle tunneling nature also makes the SymFET robust to certain quantities to which the BiSFET is sensitive. As discussed earlier, the SymFET is robust to temperature. Another advantage is the robustness of single-particle tunneling—this is an intrinsic advantage for the SymFET. Although the tunneling current will vary with the tunneling insulator thickness and its dielectric constant, the regular single-particle tunneling behavior will survive in all temperature and thickness values. Thus, unlike the BiSFET’s sensitivity to thickness variations, the SymFET behavior is robust to thickness and dielectric constant variations. Both thickness variations and inelastic scattering processes can be significantly suppressed by using 2-D crystal “insulators” such as BN or MoS₂ between the graphene layers, preferably in a rotationally aligned structure.

In summary, we have presented an analytical model to calculate the channel doping potential and I - V characteristics in a novel electronic device structure, the SymFET. The current in a SymFET flows by tunneling from one graphene layer to the other. The current is insensitive to temperature. The resonant current peak is controlled by chemical doping and applied gate bias. The on/off ratio increases with graphene coherence length and doping. The symmetric resonant peak is a good candidate for high-speed analog applications, of which frequency multiplication is an example. The resonant peak behavior can also be the framework for new digital architectures that consume much lower power than the current state-of-the-art electronic switches.

REFERENCES

- [1] A. K. Geim and K. S. Novoselov, "The rise of graphene," *Nat. Mater.*, vol. 6, no. 3, pp. 183–191, 2007.
- [2] A. H. Castro Neto and K. Novoselov, "Two-dimensional crystals: Beyond graphene," *Mater. Exp.*, vol. 1, no. 1, pp. 10–17, Mar. 2011.
- [3] S. K. Banerjee, L. F. Register, E. Tutuc, D. Reddy, and A. H. MacDonald, "Bilayer PseudoSpin Field-Effect Transistor (BiSFET): A proposed new logic device," *IEEE Electron Device Lett.*, vol. 30, no. 2, pp. 158–160, Feb. 2009.
- [4] J. P. Eisenstein, L. N. Pfeiffer, and K. W. West, "Field-induced resonant tunneling between parallel two-dimensional electron systems," *Appl. Phys. Lett.*, vol. 58, no. 14, pp. 1497–1499, Apr. 1991.
- [5] K. M. Brown, E. H. Linfield, D. A. Ritchie, G. A. C. Jones, M. P. Grinshaw, and M. Pepper, "Resonant tunneling between parallel, two-dimensional electron gases: A new approach to device fabrication using in situ ion beam lithography and molecular beam epitaxy growth," *Appl. Phys. Lett.*, vol. 64, no. 14, pp. 1827–1829, Apr. 1994.
- [6] C. R. Dean, A. F. Young, I. Meric, C. Lee, L. Wang, S. Sorgenfrei, K. Watanabe, T. Taniguchi, P. Kim, K. L. Shepard, and J. Hone, "Boron nitride substrates for high-quality graphene electronics," *Nat. Nanotechnol.*, vol. 5, no. 10, pp. 722–726, 2010.
- [7] A. S. Mayorov, R. V. Gorbachev, S. V. Morozov, L. Britnell, R. Jalil, L. A. Ponomarenko, K. S. Novoselov, K. Watanabe, T. Taniguchi, and A. K. Geim, "Direct evidence for micron-scale ballistic transport in encapsulated graphene at room temperature," *Nano Lett.*, vol. 11, pp. 2396–2399, 2011.
- [8] L. Britnell, R. V. Gorbachev, R. Jalil, B. D. Belle, F. Schedin, A. Mishchenko, T. Georgiou, M. I. Katsnelson, L. Eaves, S. V. Morozov, N. M. R. Peres, J. Leist, A. K. Geim, K. S. Novoselov, and L. A. Ponomarenko, "Field-effect tunneling transistor based on vertical graphene heterostructures," *Science*, vol. 335, no. 6071, pp. 947–950, Feb. 2012.
- [9] H. Yang, J. Heo, S. Park, H. J. Song, D. H. Seo, K.-E. Byun, P. Kim, I. Yoo, H.-J. Chung, and K. Kim, "Graphene barristor, a triode device with a gate-controlled Schottky barrier," *Science*, vol. 336, no. 6085, pp. 1140–1143, Jun. 2012.
- [10] A. C. Seabaugh and Q. Zhang, "Low voltage tunnel transistors for beyond CMOS logic," *Proc. IEEE*, vol. 98, no. 12, pp. 2095–2110, Dec. 2010.
- [11] R. M. Feenstra, D. Jena, and G. Gu, "Single-particle tunneling in doped graphene-insulator-graphene junctions," *J. Appl. Phys.*, vol. 111, no. 4, pp. 043 711-1–043 711-10, Feb. 2012.
- [12] S. Luryi, "Quantum capacitance devices," *Appl. Phys. Lett.*, vol. 52, no. 6, pp. 501–503, Feb. 1988.
- [13] K. M. Masum Habib, F. Zahid, and R. K. Lake, "Negative differential resistance in bilayer graphene," *Appl. Phys. Lett.*, vol. 98, no. 19, pp. 192 112-1–192 112-3, May 2011.
- [14] G.-H. Lee, Y.-J. Yu, C. Lee, C. Dean, K. L. Shepard, P. Kim, and J. Hone, "Electron tunneling through atomically flat and ultrathin hexagonal boron nitride," *Appl. Phys. Lett.*, vol. 99, no. 24, pp. 243 114-1–243 114-3, Dec. 2011.
- [15] C. R. Dean, A. F. Young, P. Cadden-Zimansky, L. Wang, H. Ren, K. Watanabe, T. Taniguchi, P. Kim, J. Hone, and K. L. Shepard, "Multi-component fractional quantum Hall effect in graphene," *Nat. Phys.*, vol. 7, no. 9, pp. 693–696, Sep. 2011.
- [16] H. Wang, A. Hsu, K. K. Kim, J. Kong, and T. Palacios, "Gigahertz ambipolar frequency multiplier based on CVD graphene," in *Proc. IEDM*, 2010, pp. 23.6.1–23.6.4.
- [17] H. Wang, A. Hsu, J. Wu, J. Kong, and T. Palacios, "Graphene-based ambipolar RF mixers," *IEEE Electron Device Lett.*, vol. 31, no. 9, pp. 906–908, Sep. 2010.
- [18] A. Nagashima, N. Tejima, Y. Gamou, T. Kawai, and C. Oshima, "Electronic dispersion relations of monolayer hexagonal boron nitride formed on the Ni 111 surface," *Phys. Rev. B, Condens. Matter*, vol. 51, no. 7, pp. 4606–4613, Feb. 1995.



Pei Zhao (S'08) is currently working toward the Ph.D. degree in electrical engineering at the University of Notre Dame, Notre Dame, IN, USA.



Randall M. Feenstra received the Ph.D. degree in applied physics from the California Institute of Technology, Pasadena, CA, USA.

He is currently a Professor with the Department of Physics, Carnegie Mellon University, Pittsburgh, PA, USA.



Gong Gu received the Ph.D. degree in electrical engineering from Princeton University, Princeton, NJ, USA, in 1999.

He is with the Department of Electrical Engineering and Computer Science, University of Tennessee, Knoxville, TN, USA.



Debdeep Jena received the Ph.D. degree in electrical and computer engineering from the University of California, Santa Barbara, CA, USA.

He is with the Department of Electrical Engineering, University of Notre Dame, Notre Dame, IN, USA.